Treatment of compounds and alloys in radiation hydrodynamics simulations of ablative laser loading

Damian C. Swift*
P-24 Plasma Physics, Los Alamos National Laboratory, MS E526, Los Alamos, New Mexico 87545, USA

J. Tinka Gammel
T-1, Los Alamos National Laboratory, MS B221, Los Alamos, New Mexico 87545, USA

Samuel M. Clegg
C-ADI, Los Alamos National Laboratory, MS J565, Los Alamos, New Mexico 87545, USA
(Received 2 December 2003; published 6 May 2004)

Different methods were compared for constructing models of the behavior of a prototype intermetallic compound, nickel aluminide, for use in radiation hydrodynamics simulations of shock wave generation by ablation induced by laser energy. The models included the equation of state, ionization, and radiation opacity. The methods of construction were evaluated by comparing the results of simulations of an ablatively generated shock wave in a sample of the alloy. The most accurate simulations were obtained using the "constant number density" mixture model to calculate the equation of state and opacity, and Thomas-Fermi ionization. This model is consistent with that found to be most accurate for simulations of ablatively shocked elements.

DOI: 10.1103/PhysRevE.69.056401 PACS number(s): 52.50.Jm, 07.35.+k, 62.50.+p, 42.62.Eh

I. INTRODUCTION

The intermetallic compound nickel aluminide (NiAl) is of interest as a prototype material exhibiting elastic anisotropy, for studies of the effect of a grain boundary on the propagation of a shock wave [1]. In the past, the response of material to dynamic loading was interpreted using empirical models, usually assuming homogeneous isotropic behavior. While these simple models have been found adequate to describe many bulk properties, they have contributed little to understanding of the underlying physics of processes which are highly nonlinear in the material state, such as fracture, chemical reactions, and shear bands. These phenomena are affected by heterogeneities in the material including anisotropy in response between grains of different crystal orientation, and by the presence of the grain boundaries themselves. We have performed experiments in which spatially and temporally resolved measurements were made of the velocity and displacement at the surface of NiAl samples as a shock wave arrived [2]. In order to capture the shock arrival with adequate time resolution, the TRIDENT laser was used to induce the shock wave by ablative loading of the sample; in this way, the uncertainty in arrival time associated with impact events was greatly reduced. However, in order to interpret the dynamic data and in particular the microstructure measured in recovered NiAl specimens, it is necessary to determine the loading history experienced at each point in the sample.

A logical approach is to simulate each experiment, using the measured irradiance history of the laser in radiation hydrodynamics simulations of the response of the sample. The material models must be valid for the solid material in the stress and time range explored, and also for the expanding plasma produced by the ablation process. Although considerable research has been performed on models for simulating the laser ablation of elements, very little has been published on the ablation of compounds. We have previously developed models for the response of solid NiAl and tested them against shock waves induced by the impact of flyer plates [3]. Here we describe models applicable to the plasma region of the problem, and compare them with a typical ablative loading experiment.

II. ABLATIVE LOADING EXPERIMENTS

To set the material models in context, we discuss the design of the laser-induced shock experiments and the method used to simulate them.

A. Experimental configuration

Experiments were performed using the TRIDENT facility at Los Alamos, a neodymium-glass laser with a fundamental wavelength of 1054 nm. The master oscillator was operated in nanosecond mode, in which the pulse delivered to the target was composed of up to 13 elements of 180 ps duration. The intensity of each element is controlled independently, allowing considerable flexibility in controlling the irradiance history. The infrared pulse was frequency doubled to 527 nm (green) to improve the coupling efficiency to matter. At this wavelength, the two main beams could each deliver up to ~250 J, and the third beam up to ~50 J. One of the main beams was used to drive the samples. The total energy and irradiance history were measured on each shot by extracting a small fraction of the laser drive by reflection from an uncoated window. The magnitude and time history

*Electronic address: dswift@lanl.gov: URL: http://public.lanl.gov/dswift

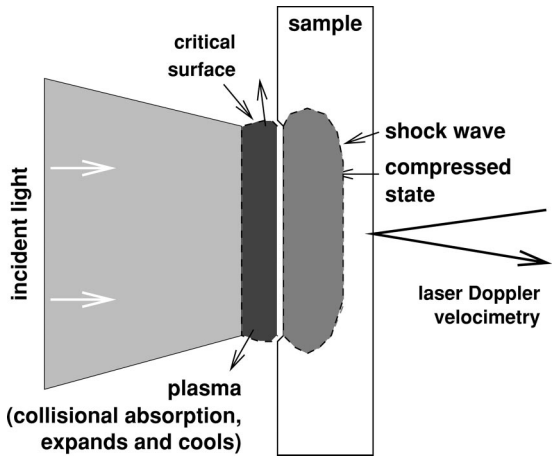

FIG. 1. Schematic cross section of laser drive experiments. Samples were 200–400 μm thick; focal spot was 5 mm in diameter.

were recorded using a calorimeter and a fast photodiode, respectively. The fractional energy measurement was calibrated to give the total energy by performing a series of experiments in which the energy reaching the center of the target chamber was measured with a second calorimeter. In this way, the total pulse energy was usually determined to ±1 J.

The raw beam from the amplifier chain had significant spatial variation. A Fresnel zone plate was used to distribute the laser energy more uniformly across the focal spot. As designed, this diffractive optical element would convert a perfectly focused spot to a disk of 4 mm diameter containing 85% of the laser light (with the remaining energy contained in higher-order rings further from the center of the disk). However, undiffracted light produced a hot spot at the center of the disk. The final focusing lens was shifted 6 mm from best focus to eliminate the hot spot; this produced a disk 5 mm in diameter. The defocusing process introduced a slight spatial variation of order 1% in irradiance, but this was not found to introduce any measurable variation in shock pressure.

In each experiment, the planar sample was irradiated on one side over a region 5 mm in diameter, and the velocity history was measured on the opposite side (Fig. 1). Each sample was an oriented crystal of NiAl, and in some experiments pairs of crystals of different orientation were exposed simultaneously to the laser drive. Samples were typically a few hundred microns thick and were wide enough to fill the region irradiated by the laser, with a margin of $\approx 1-2$ mm by which they were held in a reusable clamp. Except at the highest drive energies, the samples remained in the clamp and were recovered for postshot metallography. The use of a clamp meant that the samples were decelerated by their edges, resulting in some bending of recovered specimens. The bending was quantified during the postshot analysis by orientation-imaging electron microscopy, and was reduced in some experiments by mounting the sample against a release window to make the deceleration closer to planar.

The velocity history of the surface opposite the irradiated side was measured by laser Doppler velocimetry, using an imaging interferometer of the VISAR type [4]. Spatially distributed interference fringes were set up, and their motion recorded using two optical streak cameras. A pulsed 660 nm laser provided illumination for the VISAR. For the experiment reported here, the magnification through the VISAR system gave a field of view of 1.6 mm over 600 pixels on the charge-coupled device recording camera. The sweep period of the streak cameras was set to 16 and 37 ns, measured using a series of timing fiducials 2 ns apart. The velocity sensitivity of the VISAR was 800 m/s per fringe. The fringe pattern was converted to velocity by following the extrema as a function of time; velocity changes were thus multiplexed with position. Velocities were inferred at constant positions on the surface by interpolating between extrema. Typical velocity uncertainties were $\sim 5\%$ for an individual fringe, dominated by camera noise and diffraction rings in the optical path, which limited the accuracy of the fringe-following algorithm. The accuracy was improved by smoothing over adjacent fringes or temporal slices. Smoothing functions allowed linear variation in space or time, so the temporal resolution was not reduced significantly by this process. The time delay for light arriving through the slow leg of the interferometer was 0.4 ns, so care was taken when attempting to interpret sub-nanosecond features with this étalon.

B. Simulations

Microstructural changes such as dislocation populations and cracking were investigated by analysis of the recovered samples; the results of this analysis will be described separately. In order to interpret microstructural features in terms of the loading history experienced by the sample, the measured irradiance history was used in simulations of the laser drive process. The calculated free surface velocity history was compared with the experimental measurement to check the accuracy of the material models used in the simulations.

The simulations required radiation hydrodynamics and plasma properties to treat the ablation process, and detailed continuum mechanics incorporating single-crystal plasticity to treat shock propagation in the solid sample. These different regimes are rarely implemented in the same computer program. We used the radiation hydrocode HYADES [5] with no strength model to simulate the ablation process, and extracted the pressure history a small Lagrangian distance (initially 1 μm) from the ablation surface. The pressure history was used as an applied stress boundary condition in continuum mechanics simulations using the hydrocode LAGC [6]. The sample thickness was much less than the diameter of the laser spot, so these simulations were justifiably performed in one spatial dimension: resolving the direction through the thickness of the sample. This approach has been used previously for simulations of ablatively loaded elements [7].

In the simulations, the response of the material was represented by models for thermomechanical and transport properties. On time scales long enough that nonequilibrium effects can be ignored, these properties depend on the mass density ρ and temperature T (or specific internal energy e), and composition. Both computer programs used material

properties tabulated in the SESAME format [8], though with different units. The thermo-mechanical response was described by pressure and energy equations of state $\{p,e\}(\rho,T)$ and their derivatives; the transport properties included electrical and thermal conductivities $\{\sigma_e,\sigma_T\}(\rho,T)$ and radiation opacities (Planck and Rosseland means) $\{\sigma_P,\sigma_R\}(\rho,T)$.

The physical considerations required in constructing a material model accurate for condensed matter and for the plume of ablation plasma are different, and it is frequently difficult to construct a model valid in both regions because of the added complication of linking regions of different assumptions and approximations smoothly. In the radiation hydrodynamics simulations, the computational domain was split into a region 1 μm thick at the ablation surface in which the material models were chosen with a reasonable expectation of accuracy in the plasma regime, and a region comprising the rest of the sample in which the model of the equation of state (EOS) was chosen to be accurate in the condensed regime. In the relatively thin "ablation region," it was also desirable for the EOS to be reasonably accurate for condensed material, though greater inaccuracy could be tolerated than for the bulk of the sample.

The size of the ablation region was chosen to include more material than was actually ablated by the laser pulse, but to be thin compared with the sample itself. The amount of material ablated depends on the laser energy, the irradiance, and the nature of the material (its composition and porosity). For the regime explored here, simulations have shown that less than 1 μm of the sample is ablated; such predictions have been confirmed experimentally from the thickness or radial profile of recovered samples. Most shock wave samples used at TRIDENT have been tens to hundreds of microns thick, so 1 μm was chosen as a standard thickness for the ablation region in the simulations. Calculationally, the loading induced by ablation was thus applied first to the residual solid material in the ablation region, before being transmitted to the bulk material modeled with the more accurate solid EOS. If the plasma EOS is less accurate for the solid, there is likely to be an impedance mismatch between these two solid regions. As long as the transit time of waves in the residual ablation region is short compared with the important temporal structures in the laser pulse, pressure equilibration can occur and the states transmitted to the bulk solid should be accurate. The sensitivity to the size of the ablation region was investigated by performing simulations for thicknesses of 0.5, 1.0, and 2.0 μm. Oscillations were observed in the pressure history within the ablation region as equilibration occurred; as long as these oscillations were filtered out, the applied pressure history was the same in all cases.

III. MODELS OF ALLOY PROPERTIES

For alloys, particularly near-stoichiometric compositions, it is often the case that the EOS and elasticity can be predicted theoretically, using techniques such as *ab initio* quantum mechanics to calculate the ground state energy of the electrons and hence the relationship between pressure and compression. This was the case for NiAl, where an *ab initio* EOS was predicted and tested against shock wave experiments [3]. In contrast, accurate measurements of the EOS and transport properties of material in states relevant to the ablation plume are less readily available.

A. Continuum mixture models

A commonly used approach for predicting the properties of the vapor and plasma (and indeed the solid) is to average the properties of the constituent elements: as elements are finite in number, their properties have often been established at least approximately and are available in various forms [8,9]. With two independent variables ρ and T, the averaging of element properties for a compound or alloy can be accomplished in many different ways, i.e., through many possible mixture models. For compounds, the component atoms are intimately mixed on the scale of the simulations, so the models should represent homogeneous mixing of the species. For homogeneous mixing, the composition is specified naturally as the set of mass fractions $\{m_i\}$ or atom fractions $\{N_i\}$ of each specie i. A standard procedure used in constructing SESAME equations of state for mixtures involves models developed for heterogeneous mixtures; these models were also investigated as they were considered likely to be more accurate for condensed matter. For heterogeneous mixtures, it is meaningful to consider the composition in terms of the set of species volume fractions $\{v_i\}$, though mass fractions can be used instead. There is no particular reason why any of these models should be accurate for compounds, where the electronic structure of each component may be altered significantly from that occurring in the element. A manifestation of the electronic structure is the crystal type of the compound: NiAl adopts the CsCl structure [10], whereas pure Ni and Al are both face-centered cubic.

The heterogeneous mixture models assumed either that the compression applied to the alloy was applied equally to regions of each pure element, or that the volume fractions $\{v_i\}$ were adjusted for pressure equilibrium. The "equal pressure" model is physically more plausible, at least for a heterogeneous mixture. A homogeneous mixture model commonly used for low pressure gases is "partial pressures" [11], here extended to apply to all EOS and transport properties as well as pressure, as has been applied previously to mixed-species astrophysical plasmas [12]. In the partial pressures model, each specie is considered in turn and its mass density used to calculate a contribution to the material properties; the contribution from each component is added to predict the properties of the mixture. This model is reasonable when the mean free path of the atoms is comparable with or larger than the size of the sample; it is very inaccurate for dense samples. For plasmas of around 1% of solid density or greater, more accurate predictions were obtained by considering each specie in turn, assuming that all atoms in the material were of that type, and calculating the properties; the properties of the mixture were obtained from a weighted average using the atom fraction N_i of each specie [14]. This model is referred to as "constant number density" (Table I).

Each model was used to calculate an EOS in SESAME tabular format. The homogeneous models were used to cal-

TABLE I. Models used for constructing NiAl properties from those of constituent elements. A_i is the atomic mass of specie i. The opacity has dimensions (length)^2/(mass), so the weighting used in the constant number density model is the mass fraction rather than the atom fraction.

Model	Component state	EOS	Transport
Heterogeneous			
Equal pressure	$\rho_i : p_i(\rho_i, T)$ equal	$p = p_i \quad \forall i$	$\sigma = \Sigma m_i \sigma_i(\rho_i, T)$
Equal compression	$\rho_i = \rho \rho_{0i} / \rho_0$	$p = \Sigma v_i p_i(\rho_i, T)$	$\sigma = \Sigma m_i \sigma_i(\rho_i, T)$
Homogeneous			
Partial pressures	$\rho_i = m_i \rho$	$p = \Sigma p_i(\rho_i, T)$	$\sigma = \Sigma \sigma_i(\rho_i, T)$
Constant number density	$\rho_i = A_{ri} n$ $: n = \rho \Sigma m_i / A_{ri}$	$p = \Sigma N_i p_i(\rho_i, T)$	$\sigma = \Sigma m_i \sigma_i(\rho_i, T)$

culate opacities, again in SESAME format. A simple measure of the accuracy of each model is to calculate the mass density at standard temperature and pressure (STP). This was done using SESAME EOS for Ni (table 3101) and Al (table 3719) [8] (Table II). The equal compression model was reasonably accurate and the partial pressures model poor. All except for the partial pressures model were applied in the ablation layer of the radiation hydrodynamics simulations.

B. Constructions for specific composition

In principle a more physically justifiable and hence potentially more accurate way to proceed is to calculate properties as rigorously as possible for the specific composition of interest. This approach may be too computationally demanding if the local composition changes during the simulation, e.g., if species diffuse at significantly different rates, requiring calculations to be performed of the instantaneous mixture properties at each location in the simulation. Differential diffusion may occur at some level in the ablation plume, but was ignored in the present work.

The EOS of solid NiAl was predicted using *ab initio* quantum mechanics of the CsCl structure [3] which is the structure observed to occur at STP. This is an example of composition-specific construction, but as the quantum mechanical method predicted accurate electron ground states of a periodic lattice, it was not suitable for the low density plasma regime where the material was a tenuous, ionized fluid.

A prescription has been used to generate SESAME EOS for mixtures [8], comprising Thomas-Fermi-Dirac calculations with additive volume mixing at high compressions, shock wave data from ambient to the limit of the shock data, and average atom Lennard-Jones for the vapor region, with Grüneisen's approximation and a Debye treatment of the thermal contribution. This prescription was applied to NiAl, using the shock Hugoniot predicted from the *ab initio* quantum mechanical EOS and the observed melting temperature. The computer program used to calculate the EOS had a numerical instability in the algorithm used to make Maxwell constructions through the liquid/vapor region, normally requiring significant manual intervention to correct, so Maxwell constructions were omitted to leave van der Waals loops in the EOS [11].

The "QEOS" prescription [13] was also used. QEOS includes a set of general rules for the form of the EOS in different regimes, constructed by comparing the observed or calculated behavior of many different materials. QEOS was embedded within the HYADES program, so it was not used to generate a separate EOS for evaluation.

TABLE II. Comparison of STP mass density predicted from continuum mixture models.

Model	Mass density (g/cm^3)
Equal compression	5.997
Equal pressures	4.143
Partial pressures	10.347
Constant number density	5.182
Experiment	5.912

IV. COMPARISON OF PERFORMANCE

The different methods of calculating properties for NiAl were evaluated by comparing their performance when applied to problems exploring different aspects of their behavior. The EOS were compared first against shock wave data, which involves only the mechanical response with no contribution from transport properties in the regime considered. The combined mechanical and transport behavior was compared through simulations of the material pressure induced near the drive surface by laser ablation. The combined properties were also investigated by comparing against free surface velocity data from laser ablation experiments on relatively thick samples in which the shock wave decayed before reaching the free surface.

A. Principal shock Hugoniot

The EOS were used to calculate the principal shock Hugoniot — the locus of states reached from the STP state by the passage of a shock wave of a given strength — by solving the Rankine-Hugoniot relations for the conservation of mass, momentum, and energy across a steady shock wave [15]:

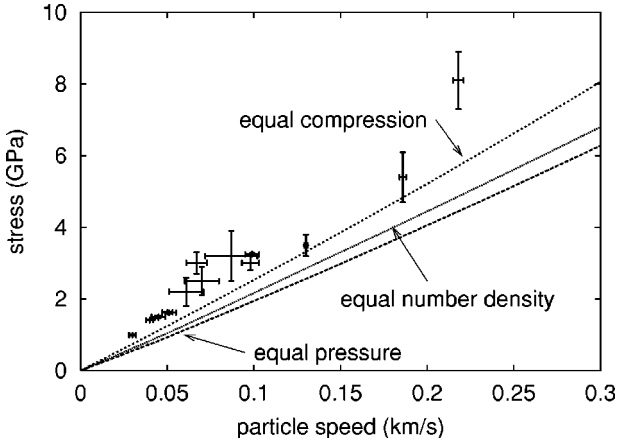

FIG. 2. Comparison between principal shock Hugoniot predicted using different continuum mixture models and flyer impact data.

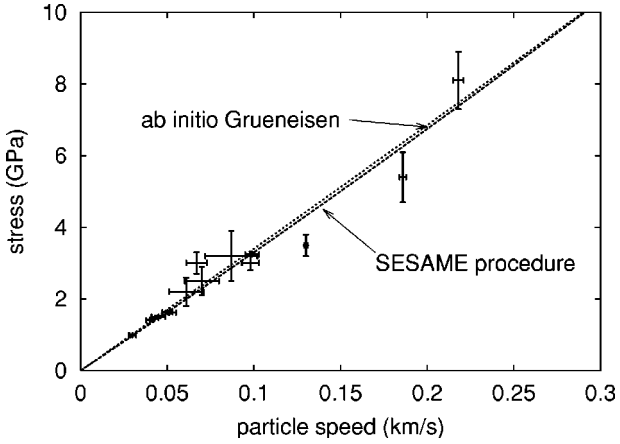

FIG. 3. Comparison between principal shock Hugoniot predicted using *ab initio* quantum mechanics, SESAME procedure incorporating *ab initio* Hugoniot, and flyer impact data.

$$u_s^2 = v_0^2 \frac{p - p_0}{v_0 - v}, \tag{1}$$

$$u_p = \sqrt{[(p - p_0)(v_0 - v)]}, \tag{2}$$

$$e = e_0 + \tfrac{1}{2}(p + p_0)(v_0 - v), \tag{3}$$

where u_s is the shock speed and u_p the piston or particle speed of material behind the shock with respect to the unshocked material, and $v = 1/\rho$ is specific volume. Bilinear interpolation was used to interpret the tabular EOS. The partial pressure EOS was not used, because its mass density at STP was insufficiently accurate. The shock Hugoniots were compared with experimental data, obtained from flyer impact experiments [3].

All of the continuum mixture models were significantly softer than the experimental data (Fig. 2). The equal compression model was the best and the equal pressure the worst. As reported previously [3], the *ab initio* quantum mechanical model passed within the estimated uncertainty of almost every experimental point, and notable within all the points of smallest error. The EOS constructed according to the SESAME prescription matched the *ab initio* EOS to high accuracy, as it should since the shock Hugoniot from the latter was used in the construction of the EOS (Fig. 3).

The comparison of shock Hugoniots demonstrates the importance of an accurate treatment of the electronic structure, and the degree to which it changes between heterogeneous mixtures and the formation of intermetallic compounds. It is also interesting to note that, of the heterogeneous continuum mixture models, the model apparently containing more physics was less accurate: this demonstrates the importance of including the correct physics.

B. Pressure-irradiance relation for laser ablation

A simple measure of the response of a material to irradiation by a laser is to calculate relations between the laser irradiance and the pressure induced in the material. A laser pulse of constant irradiance does not generally induce a constant shock pressure, but it was found previously for nanosecond duration pulses on elements that a region of relatively slowly varying pressure was produced behind an initial pressure spike [7]. The experiments on NiAl used samples which were too thick to allow this pressure to be determined directly, e.g., from the free surface velocity, but radiation hydrodynamics simulations of the pressure-irradiance relation are a useful way to compare different sets of models.

The initial spatial mesh in HYADES was set up to increase geometrically, to allow adequate resolution of the material to be ablated. The cell closest to the surface was 5 nm wide; successive cells were expanded by 5% moving away from the surface. This resolution was found previously [7] to give numerically converged shock profiles in the condensed sample. The flux limiter was set to 0.03 of the free stream value — a common choice for simulations of this type [16]. The irradiance was ramped up and down over 0.1 ns to maintain stability in the simulations.

The EOS in the ablation region was modeled by each of the mixture EOS described above; the EOS in the bulk solid material was the *ab initio* quantum mechanical construction. Opacities for radiation diffusion were again modeled using the mixture models. Conductivities for laser deposition and heat conduction were calculated using several different ionization models: Saha, Thomas-Fermi, and average atom [5,8,18].

Similar computational studies on ablative loading of elements indicated that radiation transport could be omitted for elements of atomic number up to that of Fe at least, giving simulations with the same temperature for ions, electrons, and radiation [17]. To reduce the number of alternative material models to evaluate at once, the base line model chosen for sensitivity studies comprised QEOS for the EOS and Thomas-Fermi ionization. The sensitivity to EOS was then investigated by comparing pressure-irradiance relations with the mixture model EOS substituted in the ablation region. Problems were encountered with the mixture EOS constructed according to the SESAME prescription, the van der Waals loops causing imaginary sound speeds which halted the simulation. The pressure-irradiance relations for NiAl

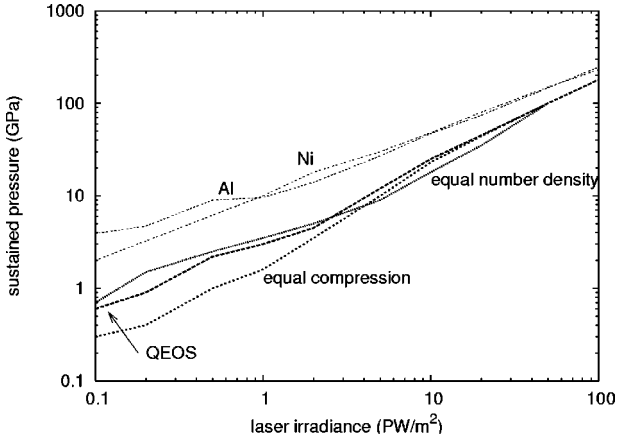

FIG. 4. Comparison between irradiance-pressure relations predicted for NiAl using Thomas-Fermi ionization, no radiation transport, and different equations of state.

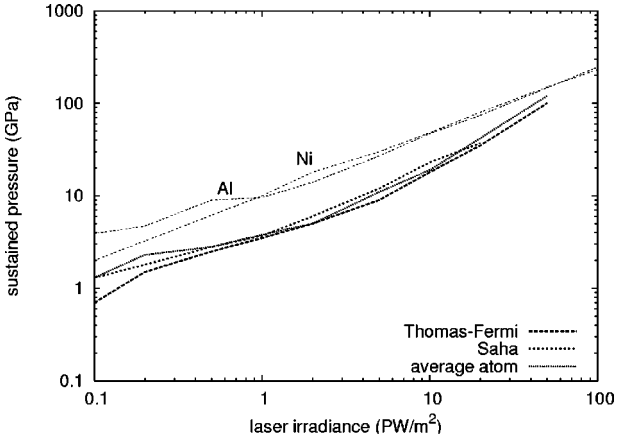

FIG. 5. Comparison between irradiance-pressure relations predicted for NiAl using the constant number density mixture equation of state and no radiation transport, for different ionization models.

were compared with the relations calculated for elemental Ni and Al. One would expect the relation for NiAl to differ somewhat from that of its constituent elements, but not to deviate very far. The relation for Al was validated previously by comparing radiation hydrodynamics simulations with the velocity history measured at the free surface of thin (25 μm) foils. The relation for Ni was not tested experimentally, but was similar to that for Fe, which was tested in the same way as for Al. All of the alloy simulations gave relations which were significantly lower in pressure than that for Ni and Al over most of the irradiance range considered, though the relations converged for high irradiance. The relation from the equal compression EOS was significantly lower than that from the other two EOS, which were reasonably consistent with each other (Fig. 4).

Simulations were then made using the constant number density EOS and no radiation transport, changing the ionization model used to calculate conductivities. The pressure-irradiance relations were fairly similar with Thomas-Fermi, Saha, or average atom ionizations. Again, all were significantly lower than the relations calculated for elemental Ni and Al over most of the irradiance range but converged at high irradiance (Fig. 5).

Finally, simulations were performed using the constant number density EOS and Thomas-Fermi ionization, and opacity calculated using the partial pressures or constant number density model. Incorporating radiation transport by the inclusion of either opacity model brought the pressure-irradiance relation predicted for NiAl much closer to that for Ni and Al (Fig. 6).

Based on this sensitivity study, the most plausible representation for the properties of NiAl in the ablation region of radiation hydrodynamics simulations was Thomas-Fermi ionization, and EOS and opacity calculated using the constant number density model. The pressure-irradiance relation was not very sensitive to the substitution of Saha or average atom calculations of the ionization, nor to the use of QEOS or the equal pressures mixture model for the EOS. However, Thomas-Fermi ionization was found to be accurate over a wider range of atomic numbers and states than the other ionization models when applied to elements, and the constant number density model allows both the EOS and opacity to be calculated self-consistently. This model is also computationally efficient, which may be important for future studies in which species are permitted to diffuse at different rates.

C. TRIDENT shot 15405

A more direct test of the accuracy of the models is to simulate the velocity history at the free surface of a sample of NiAl subjected to ablative loading. TRIDENT shot 15405 was chosen; the target comprised two crystals of NiAl mounted side by side: one cut with its surface parallel to (100) and the other parallel to (110). The crystals were 267 and 266 μm thick, respectively. The field of view of the VISAR and streak camera were set to record the arrival of the shock wave in both samples (Fig. 7).

These samples were hydrodynamically thick, in the sense that the transit time of the shock wave through the sample was long compared with the duration of the laser pulse. After

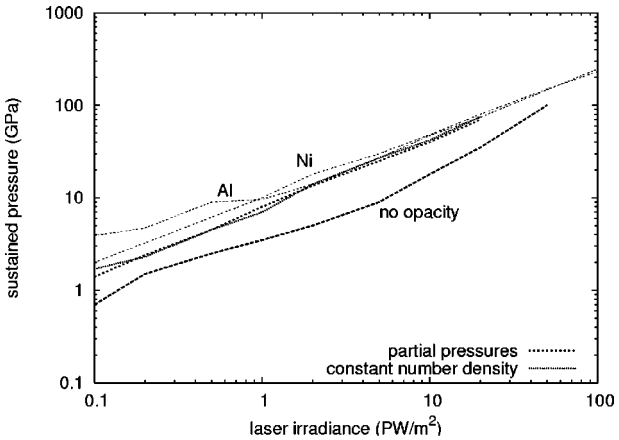

FIG. 6. Comparison between irradiance-pressure relations predicted for NiAl using the constant number density mixture equation of state and Thomas-Fermi ionization, for different opacity models. The curves for partial pressures and constant number density opacity models are close to one another.

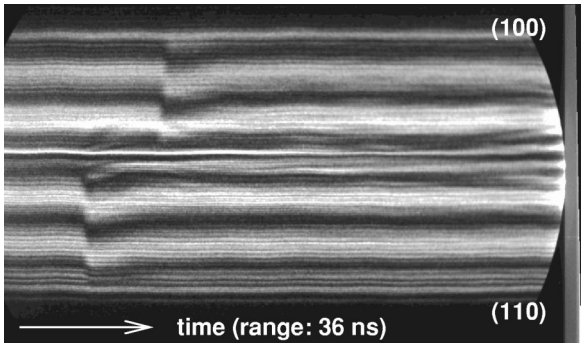

FIG. 7. Line VISAR record from TRIDENT shot 15405, showing fringe displacement (corresponding to velocity change) as shock waves reached the surface in NiAl crystals of different orientation. One complete fringe displacement equates to an acceleration of 800 m/s. The field of view was ≈1.6 mm wide.

the end of the laser pulse, the plasma plume expands and dissipates, and a rarefaction propagates from the ablation surface, relieving the stress induced by the ablative loading, and usually traveling faster than the shock. In thick samples, the rarefaction can overtake the shock before it reaches the opposite surface of the sample, causing the shock to decay in amplitude as it propagates further through the sample. For a weak or decaying shock, the constitutive properties of the material should be included in simulations, as well as the EOS. The flyer impact experiments performed to test the EOS also allowed the plastic flow properties to be estimated for crystals cut in the (100) orientation [3]. Thus only the (100) sample from shot 15405 was selected for detailed simulations.

The irradiance history delivered to the sample was inferred from beam measurements to be around 0.1 PW/m^2 (Fig. 8). The irradiance history was simplified slightly to remove small-scale oscillations which can sometimes cause numerical problems, and was applied in the radiation hydrodynamics simulation. We have found previously that filtering out features shorter than 200 ps or so in the irradiance history has little effect on the state in the sample at depths

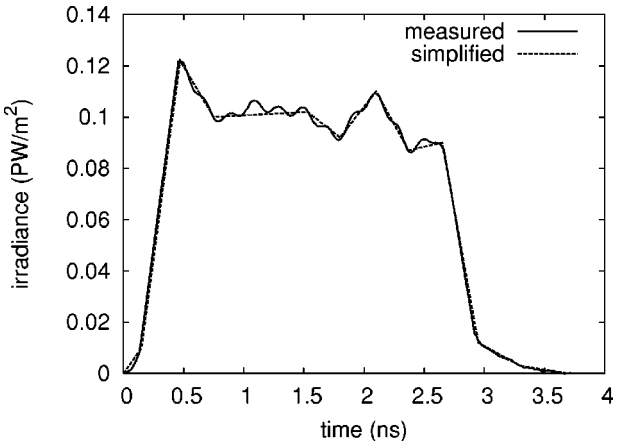

FIG. 8. Irradiance history applied to NiAl (100) sample in TRIDENT shot 15405, and simplified irradiance history used in radiation hydrodynamics simulations.

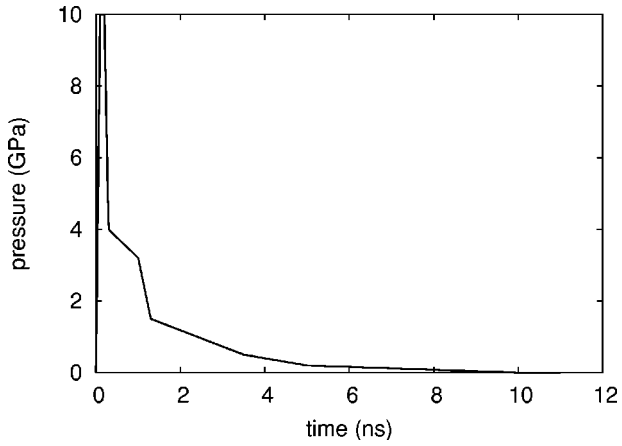

FIG. 9. Pressure history predicted to occur 1 μm from the ablation surface in TRIDENT shot 15405, simplified for use as boundary condition in continuum mechanics simulation.

greater than a few microns. With samples as thick as the NiAl crystals, the effect on the free surface velocity history was negligible. From the radiation hydrodynamics simulations, the pressure history was estimated 1 μm into the sample. At these relatively low irradiances, the simulated pressure history exhibited some spikes and high frequency oscillations, probably caused by the sequential ablation of individual computational zones. Again, unphysical features were smoothed out of the history before using it as a boundary condition for subsequent calculations (Fig. 9).

The calculated pressure history was used as a time-dependent applied pressure boundary condition for continuum mechanics simulations of the sample, incorporating an elastic-plastic model for the constitutive response of NiAl in the (100) direction. Because the shock was decaying, the structure around the shock peak was sensitive to mesh resolution, particularly on the rising edge of the shock. A zone size of 0.5 μm was found to give a converged peak velocity and a reasonably short shock rise time. These simulations were used to predict the free surface velocity history. Using the set of models deduced above to be appropriate for ablative loading of a compound, the velocity history agreed well with the peak velocity and duration of the velocity excursion measured using the line VISAR on shot 15405 (Fig. 10). There was some uncertainty in the absolute timing calibration on these thick samples because the train of fiducial pulses had decayed to a level too low to be visible before the arrival of the shock wave, so for purposes of comparison the experimental record was shifted in time to match the arrival time in the simulation. The experimental record exhibited small-amplitude oscillations in velocity which were artefacts of the particular streak camera used. The experimental record also exhibited a decrease in deceleration at the end of the shock event, resulting in a higher velocity at late times than in the simulation. This difference is probably caused by spall or tensile damage in the sample; spall was neglected in these simulations.

V. CONCLUSIONS

A method was devised for simulating ablative laser loading experiments on alloys and compounds, for which the

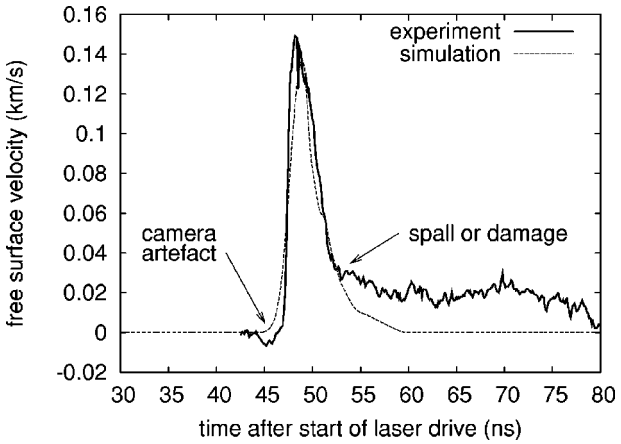

FIG. 10. Comparison between predicted and measured free surface velocity history for TRIDENT shot 15405.

equation of state and transport properties may not be well established in the plasma regime. The computational domain of the sample material was split into a thin region at the ablation surface in which the material was represented using the best available plasma model, and the bulk of the sample in which the best available condensed phase model was used. The model used in the ablation region should also exhibit reasonable behavior for condensed material: an initial density and shock compressibility accurate to of order 10%.

Radiation hydrodynamics simulations otherwise used the same models as were found previously to be valid for elements in the same regime: laser pulses of order nanosecond duration and irradiance 0.1 to 100 PW/m^2, giving sustained pressures between ~ 1 and 100 GPa. The models included Thomas-Fermi ionization for calculating conductivities and three temperature hydrodynamics (ion, electron, and radiation) in the plasma plume. The simulations were more sensitive to the inclusion or omission of radiation transport than was found for elements.

Several mixture models were investigated for the intermetallic compound NiAl, intended primarily for the plasma region. All were somewhat too soft when used to predict the equation of state of solid NiAl, underscoring the need to split the computational domain into "mainly ablated" and "never ablated" regions. The best simulations were obtained using the constant number density mixture model for the equation of state and radiation opacity. Significant variation was found when using different mixture models, or when neglecting radiation transport.

Detailed simulations of the ablative loading of a NiAl crystal were performed. Using the radiation hydrodynamics model developed above, the predicted velocity history at the free surface of the sample was in good agreement with experimental data.

ACKNOWLEDGMENTS

Ken McClellan, John Brooks, and Darrin Byler (MST-8) prepared the NiAl samples. Tom Tierney (P-24) helped to set up the TRIDENT experiments. The staff of TRIDENT contributed greatly to the conduct of the experiments. Pedro Peralta and Eric Loomis (Arizona State University) performed postshot metallography of the recovered samples. J.D. Johnson (T-1) provided help with the suite of software used to generate SESAME tables, and Jon Larsen (Cascade Applied Sciences, Inc.) gave advice on the use of HYADES. Thanks are due to Carter Munson (P-24) for his careful review of the manuscript, and to the anonymous journal reviewer for helpful suggestions. Funding for this work was provided by LANL's Science and Technology Base Programs Office through Laboratory-Directed Research and Development (Directed Research) Project No. 2002-087, "New Windows into Shocks at the Mesoscale," Principal Investigator Aaron Koskelo (C-ADI). Support was also provided by the LANL Program Office for the National Nuclear Security Administration's Campaign 10, by the provision of time on the TRIDENT facility. The work was performed under the auspices of the U.S. Department of Energy under Contract No. W-7405-ENG-36.

[1] A. C. Koskelo, S. R. Greenfield, D. Greening, and D. C. Swift, in *Shock Compression of Condensed Matter-2003*, edited by M. D. Furnish, Y. M. Gupta, and J.. Forbes, AIP Conf. Proc. No. 804 (AIP, Melville, NY, 2004).

[2] S. R. Greenfield, D. C. Swift, and A. C. Koskelo, in *Shock Compression of Condensed Matter-2003* (Ref. [1]).

[3] K. J. McClellan, D. C. Swift, D. L. Paisley, and A. C. Koskelo, in *Shock Compression of Condensed Matter-2003* (Ref. [1]).

[4] L. M. Barker and R. E. Hollenbach, J. Appl. Phys. **43**, 4669 (1972).

[5] Documentation for HYADES computer program, version 01.05.11 (Cascade Applied Sciences Inc., Golden, Colorado, 1998).

[6] Documentation for LAGC computer program version 0.2 (incorporating ARIADNE material properties library, version 7.0, and C++ mathematical class library, version 1.2) (Wessex Scientific and Technical Services Ltd., Perth, Scotland, 2003; http://www.wxres.com).

[7] D. C. Swift, T. E. Tierney, R. A. Kopp, and J. T. Gammel Phys. Rev. E **69**, 036406 (2004).

[8] S. P. Lyon and J. D. Johnson (Los Alamos National Laboratory), "SESAME: the Los Alamos National Laboratory equation of state database," Los Alamos National Laboratory Report No. LA-UR-92-3407, 1992 (unpublished).

[9] D. J. Steinberg, "Equation of State and Strength Properties of Selected Materials," Lawrence Livermore National Laboratory Report No. UCRL-MA-106439, 1996 (unpublished).

[10] D. B. Miracle, Acta Metall. Mater. **41**, 649 (1993).

[11] J. R. Waldram, *The Theory of Thermodynamics* (Cambridge University Press, Cambridge, 1985).

[12] R. Bowers and T. Deeming, *Astrophysics I: Stars* (Jones and Bartlett, Boston, 1984).

[13] R. M. More, K. H. Warren, D. A. Young, and G. B. Zimmerman, Phys. Fluids **31**, 10 (1988).
[14] D. C. Swift (unpublished).
[15] A. V. Bushman, G. I. Kanel', A. L. Ni, and V. E. Fortov, *Intense Dynamic Loading of Condensed Matter* (Taylor & Francis, London, 1993).
[16] R. Dendy, *Plasma Physics* (Cambridge University Press, Cambridge, 1993).
[17] D. C. Swift, D. L. Paisley, A. Forsman, J. Niemczura, T. E. Tierney, R. P. Johnson, G. A. Kyrala, and A. Hauer, in *Fifth International Symposium on High Dynamic Pressures*, edited by J. Vanpoperynghe (Centre d'Études Atomiques, Paris, 2003), Vol. 2, pp. 343–351.
[18] Ya. B. Zel'dovich and Yu. P. Raizer, *Physics of Shock Waves and High Temperature Hydrodynamic Phenomena* (Academic Press, New York, 1966).